

Tunable Anomalous Diffusion in Subrecoil-Laser-Cooled Atoms

Soma Shiraki,¹ Eli Barkai,² and Takuma Akimoto^{1,*}

¹*Department of Physics and Astronomy, Tokyo University of Science, Noda, Chiba 278-8510, Japan*

²*Department of Physics, Bar-Ilan University, Ramat-Gan, Israel*

(Dated: March 20, 2025)

The control of atomic motion through laser cooling has revolutionized quantum technologies, enabling applications ranging from quantum computing to precision metrology. However, the spatial spreading of subrecoil-laser-cooled atoms—crucial for understanding cooling mechanisms and atomic confinement—remains largely unexplored. Here, we analyze anomalous diffusion in subrecoil-laser-cooled atoms, where a velocity-dependent fluorescence rate $R(v) \propto |v|^\alpha$ governs transport properties. By tuning α , we uncover transitions between normal, subdiffusive, and superdiffusive regimes. Notably, at $\alpha = 3/2$, diffusion is minimized, leading to optimal atomic confinement. These findings advance the understanding of anomalous transport in laser-cooled systems and offer new avenues for precise control of atomic motion.

Laser cooling techniques have revolutionized atomic motion control, driving advances in both fundamental physics and applied technologies, including quantum computing and precision metrology [1–10]. These methods have enabled the exploration of ultracold gases, leading to the realization of Bose-Einstein condensation [11, 12], where quantum effects manifest on a macroscopic scale, opening new avenues in many-body physics and quantum simulations [13].

In these systems, laser fields replace the conventional thermal heat bath, leading to behaviors that deviate significantly from the predictions of standard statistical physics [7, 14, 15]. These deviations persist while the laser remains active, maintaining the system out of equilibrium. Subrecoil laser cooling enables nanokelvin temperatures by exploiting a velocity-dependent fluorescence rate that scales as $R(v) \propto |v|^\alpha$ for small velocities v [16–18]. This cooling mechanism allows for the spreading of a packet of atoms, which can be directly measured in experiments. The shape of this packet is strongly influenced by the cooling process. Importantly, the velocity-dependent rate suppresses laser-atom interactions in the low-velocity limit ($v \rightarrow 0$), effectively slowing atomic motion. Efficient cooling is achieved when $\alpha > 1$, as the mean lifetime of atoms in the “dark state”—where at low velocities they effectively cease interacting with the laser—diverges [14]. This divergence fundamentally transforms the system’s dynamics, disrupting classical concepts of equilibrium and diffusion. Consequently, this unique mechanism facilitates the accumulation of ultracold atoms with non-thermal velocity distributions [14, 19], as observed in experiments [16, 20–25].

A central challenge in subrecoil-laser cooling is understanding atomic diffusion, which governs both cooling efficiency and positional stability. The fundamental question remains: What is the nature of this diffusion—normal, subdiffusive, or superdiffusive? Here, we investigate the diffusion dynamics in subrecoil-laser-cooled systems using fundamental stochastic models of subrecoil-laser cooling [14, 16]. In these models, the

time interval between successive velocity changes, known as the flight time, is a key stochastic variable. At low speeds, these intervals are exceptionally long and follow a fat-tailed distribution. Such broad-tailed flight times, within the well-known Lévy walk approach, are a characteristic typically associated with superdiffusion [26–34]. However, as we show below, under certain conditions, the non-trivial coupling between these prolonged flight times and flight lengths results in subdiffusion instead. [35–40].

Since the parameter α is tunable in experiments, a key question is: What value minimizes diffusion? This is crucial for stabilizing the spreading atomic packet. As we show below, a non-trivial value, $\alpha = 3/2$, leads to the slowest diffusion, maximizing atomic stability. These findings highlight the role of α in controlling transport dynamics. Moreover, they offer a fundamental understanding of anomalous diffusion in subrecoil-laser-cooled systems, laying the groundwork for future advancements in atomic control.

Models.—To capture the essential physics of subrecoil laser cooling, we first adopt the stochastic framework and consider two well-established models introduced by Bardou et al.: the rate-induced Lévy walk (RILW) and the inhomogeneous random walk (IRW) [14]. The RILW model assumes that velocities are independently randomized, neglecting correlations between successive emissions, while the IRW model retains these correlations [14]. In subrecoil laser cooling, atomic velocity evolves through stochastic photon emission and absorption, effectively modeled as a one-dimensional random-walk process with a velocity-dependent jump rate $R(v)$ [14, 41].

In the IRW model, velocity updates occur as $v_1 = v_0 + \Delta v$, where v_0 is the initial velocity, v_1 is the post-collision velocity, and Δv is drawn from a Gaussian distribution with mean zero and variance σ^2 . This model captures the correlation between velocity steps, introducing memory effects in atomic motion. To stabilize the cooling dynamics, we impose reflecting boundaries at $|v| = v_{\max}$, confining the velocity within the physically meaningful range $[-v_{\max}, v_{\max}]$. This condition reflects

experimental setups, which constrain the maximal speed of the atomic motion [17, 42]. The RILW model, on the other hand, adopts a coarse-grained approach: since multiple spontaneous emissions decorrelate atomic velocity, post-collision velocities are drawn from independent and identically distributed (IID) random variables following a stationary symmetric distribution $f(v)$.

In both models, collisions occur at random intervals, where flight times, conditioned on the velocity v , follow an exponential distribution. Later, we will show that when this velocity dependence is removed, the flight-time distribution exhibits a power-law tail. The fluorescence rate $R(v)$ [14], which determines the inverse of the mean flight time, is given by

$$R(v) = \frac{1}{\tau_0} \left| \frac{v}{v_r} \right|^\alpha. \quad (1)$$

Here, α controls the velocity dependence of the jump rate, and v_r is a characteristic velocity scale for the cooling process. As $v \rightarrow 0$, interactions between atoms and the laser field cease, leading to vanishing jumps. Experimental setups, such as velocity-selective coherent population trapping, typically use $\alpha = 2$ or 4 to restrict atomic speeds to small values [43, 44]. The parameter τ_0 corresponds to the characteristic photon emission timescale, setting the rate of interaction with the cooling laser [14, 18]. For simplicity, we set $v_r = 1$ and $\tau_0 = 1$ in our analysis.

During a flight, an atom moves at a constant velocity for a random flight time, after which its velocity changes, resembling the dynamics of a Lévy walk (see Fig. 1). However, unlike a Lévy walk, the probability density function (PDF) of flight times depends on velocity v and follows an exponential distribution with a mean flight duration of $1/R(v)$. However, since v evolves stochastically throughout the process, the overall flight time distribution exhibits power-law-like behavior; see Eq. (5) below. Physically, these long flights occur predominantly at low speeds, where jump rates are small. This velocity-dependent jump rate plays a crucial role in determining the transport regime, including possible anomalous diffusion. Furthermore, in the IRW model, correlated velocity changes between collisions violate the renewal assumption of Lévy walks, introducing additional complexity into the diffusion process.

For analytical tractability, we first focus on the RILW model [14], where velocity changes are uncorrelated. The master equation governing the velocity distribution $\rho(v, t)$ in the RILW model is given by

$$\frac{\partial \rho(v, t)}{\partial t} = -R(v)\rho(v, t) + \int_{-1}^1 R(v')\rho(v', t)f(v)dv', \quad (2)$$

where v represents the velocity immediately after a jump, and $R(v)$ and $f(v)$ are as defined earlier. This equation describes the evolution of the velocity distribution,

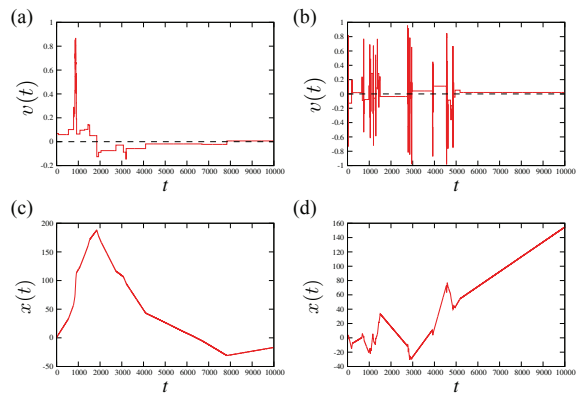


FIG. 1. Trajectories of velocity and position in the IRW and RILW models for $\alpha = 2$, which exhibit a fractal-like behavior with power-law flight times, somewhat similar to Lévy walks. (a), (b) Velocity trajectories in the IRW and RILW models, respectively. (c), (d) Corresponding position trajectories for (a) and (b), respectively. In the IRW model, velocity updates retain the memory of prior states, in contrast to the RILW model, where velocity resets independently after each step. Despite this difference, both models yield statistically equivalent diffusion properties.

where the first term accounts for velocity changes due to jumps, and the second term represents the redistribution of velocities according to $f(v)$, reflecting the stochastic nature of the process. To illustrate our key results, we set $f(v) = 1/2$ for $-1 < v < 1$ otherwise $f(v) = 0$.

At long times, the velocity distribution evolves as

$$\lim_{t \rightarrow \infty} Z(t)\rho(v, t) = f(v)|v|^{-\alpha}, \quad (3)$$

where $\rho(v, t)$ is the normalized density, and $Z(t)$ is a time-dependent normalization factor [16, 19]. For $\alpha < 1$ and $f(0) \neq 0$, $Z(t)$ becomes constant as $t \rightarrow \infty$, indicating a steady-state solution. In contrast, for $1 \leq \alpha$, $Z(t)$ grows as $Z(t) \propto t^{1-\alpha-1}$, signifying the absence of a conventional steady state. As we will show below, $\alpha = 1$ also marks a transition in the spatial spreading of particles.

In the RILW model, the position of an atom starting at $x = 0$ evolves through a series of stochastic flights. Each flight duration τ is exponentially distributed with a mean $1/R(v)$. During each flight, the atom moves at a constant velocity, resulting in a displacement $\Delta x = v\tau$. At the end of the flight, the velocity is updated to a new value sampled from the distribution $f(v)$, and the process repeats. Using Eq. (1), the joint PDF $\psi(\Delta x, \tau)$ of displacement Δx and flight time τ is given by

$$\psi(\Delta x, \tau) = \int_{-1}^1 \frac{dv}{2} |v|^\alpha e^{-|v|^\alpha \tau} \delta(\Delta x - v\tau). \quad (4)$$

The flight-time distribution $\phi(\tau)$ is given by integrating Eq. (4) over Δx :

$$\phi(\tau) = \frac{\gamma(\frac{1}{\alpha} + 1, \tau)}{\alpha} \tau^{-1-\frac{1}{\alpha}}, \quad (5)$$

where $\gamma(\cdot, \tau)$ denotes the incomplete gamma function. For large time τ , the flight-time distribution asymptotically behaves as $\phi(\tau) \sim \frac{1}{\alpha} \Gamma(\frac{1}{\alpha} + 1) \tau^{-1 - \frac{1}{\alpha}}$. Thus, the mean flight time remains finite for $\alpha < 1$ but diverges for $\alpha > 1$. We also use the Laplace transform, given by $\hat{\phi}(s) = 1 - as^{\frac{1}{\alpha}} + o(s^{\frac{1}{\alpha}})$ for $\alpha > 1$, where $a = \pi \csc(\pi/\alpha)/\alpha$. This small s expansion of $\hat{\psi}(s)$ is non-analytical, which reflects the fact that the mean flight time diverges.

The flight-displacement distribution $\varphi(\Delta x)$ is obtained by the marginal distribution of Eq. (4), which yields

$$\varphi(\Delta x) = \frac{|\Delta x|^{-\frac{\alpha}{\alpha-1}}}{2(\alpha-1)} \gamma\left(\frac{1}{\alpha-1}, |\Delta x|\right). \quad (6)$$

For large displacements, the flight-displacement distribution behaves asymptotically as

$$\varphi(\Delta x) \sim \frac{\Gamma(\frac{1}{\alpha-1})}{2(\alpha-1)} |\Delta x|^{-1 - \frac{1}{\alpha-1}} \quad (|\Delta x| \rightarrow \infty). \quad (7)$$

Thus, the mean flight length $\langle |\Delta x| \rangle$ diverges for $\alpha \geq 2$, while the second moment $\langle \Delta x^2 \rangle$ diverges for $\alpha \geq 3/2$. Naively, one might expect that since the variance of the jump length diverges at $\alpha = 3/2$, the system should exhibit superdiffusion. However, as we show below, this expectation is incorrect. Instead, $\alpha = 3/2$ marks the regime of slowest dispersion, which arises due to the coupling between jump size and flight time.

Anomalous Diffusion: Normal, Subdiffusion, and Superdiffusion.—To understand the anomalous diffusion of laser-cooled atoms, we derive the mean square displacement (MSD) $\langle x^2(t) \rangle$ using the Montroll-Weiss equation [45–47], which relates the propagator $p(x, t)$ to the jump length and waiting-time distributions. The propagator can be expressed as

$$p(x, t) = \int_{-\infty}^{\infty} d\Delta x \int_0^{\infty} d\tau Q(x - \Delta x, t - \tau) \Psi(\Delta x, \tau), \quad (8)$$

where $Q(x, t) dx dt$ represents the probability of a random walker arriving at position x at time t after completing a jump, and $\Psi(\Delta x, \tau)$ represents the PDF of the displacement during the last flight, conditioned on the fact that the flight has lasted at least τ but is not yet completed. Since an atom with velocity v remains in that state for a duration τ with probability $e^{-|v|\alpha\tau}$, the corresponding displacement distribution is given by

$$\Psi(\Delta x, \tau) = \int_{-1}^1 \frac{dv}{2} e^{-|v|\alpha\tau} \delta(\Delta x - v\tau). \quad (9)$$

This function describes the distribution of jump sizes occurring between the last collision event and the measurement time t . Equation (8) is a convolution equation, which can be solved using the Fourier transform ($x \rightarrow k$) and the Laplace transform ($t \rightarrow s$). The Fourier-Laplace

transform yields the Montroll-Weiss equation [45, 48]:

$$\hat{p}(k, s) = \frac{\hat{\Psi}(k, s)}{1 - \hat{\psi}(k, s)}. \quad (10)$$

This equation explicitly yields the Laplace transform of the moments:

$$\langle \hat{x}^{2n}(s) \rangle = (-1)^n \left. \frac{\partial^{2n}}{\partial k^{2n}} \hat{p}(k, s) \right|_{k=0}, \quad (11)$$

where $\langle \hat{x}^{2n}(s) \rangle$ denotes the Laplace transform of $\langle x^{2n}(t) \rangle$ with respect to time t .

In the long-time limit, the leading-order behavior of the MSD is governed by the exponent α in the jump rate $R(v)$. The MSD reveals distinct scaling regimes dictated by the parameter α . Using Eqs. (10), (11) and Tauberian theorems, we obtain the asymptotic behavior of the MSD, which scales as $\langle x(t)^2 \rangle \propto t^{\gamma(\alpha)}$ for $t \rightarrow \infty$. The power-law exponent $\gamma(\alpha)$ is given by

$$\gamma(\alpha) = \begin{cases} 1 & (\alpha < 1) \\ \frac{1}{\alpha} & (1 < \alpha < \frac{3}{2}) \\ 2 - \frac{2}{\alpha} & (\alpha > \frac{3}{2}). \end{cases} \quad (12)$$

The exponents in Eq. (12) differ from those in the classical Lévy walk model [32], where only superdiffusion occurs, whereas our model exhibits a broader range of diffusion behaviors, including subdiffusion. For $\alpha < 1$, the MSD increases linearly with time, indicating normal diffusion. For $1 < \alpha < 2$, subdiffusion is observed. In particular, for $1 < \alpha < 3/2$, it is characterized by a sub-linear growth of the MSD, i.e., $\langle x^2(t) \rangle \propto t^{1/\alpha}$. More precisely, in this regime, the asymptotic behavior of the MSD becomes

$$\langle x^2(t) \rangle \sim \frac{\langle \Delta x^2 \rangle}{a\Gamma(1 + \frac{1}{\alpha})} t^{\frac{1}{\alpha}}, \quad (13)$$

where $\langle \Delta x^2 \rangle$ is the second moment of the flight displacement, see Eq. (6). Subdiffusion persists for $\alpha < 2$. At $\alpha = 2$, normal diffusion is recovered, followed by the onset of superdiffusion for $\alpha > 2$. The exact asymptotic behavior for $\alpha > 3/2$ reads

$$\langle x^2(t) \rangle \sim \frac{2(\alpha - 3) \sin(\frac{\pi}{\alpha}) \csc(\frac{3\pi}{\alpha})}{\alpha\Gamma(3 - \frac{2}{\alpha})} t^{2 - \frac{2}{\alpha}}. \quad (14)$$

As α approaches $3/2$, the prefactor in Eqs. (13) and (14) diverges [see Eq. (6)]. However, the slowest diffusion pattern is found for $\alpha = 3/2$ because the subdiffusive exponent is minimized at this point (see Fig. 2). For $\alpha > 2$, the system enters a superdiffusive regime, where the MSD scales as $\langle x^2(t) \rangle \propto t^{2 - \frac{2}{\alpha}}$.

A basic question is whether similar behavior is found for the IRW model, where the collisions process exhibits

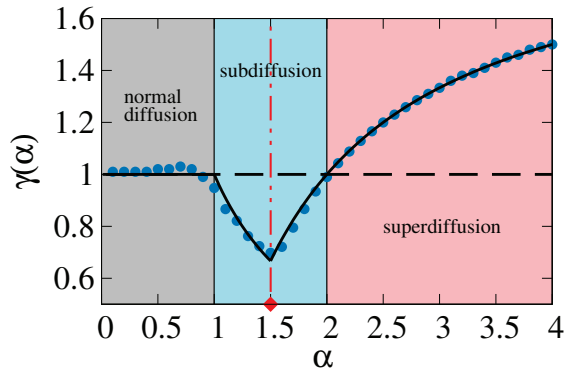


FIG. 2. Power-law exponent of the MSD as a function of α exhibiting transitions between normal, sub-, and superdiffusion. Symbols are the numerical results in the IRW model. Solid lines represent the theory of the power-law exponent for the RILW model in Eq. (12). To determine the scaling exponent in numerical simulations, we used the final decade of the observation time for fitting, and the slope obtained from this fitting is adopted as the representative value for the analysis.

correlations. We perform numerical simulations of the IRW model and compare the results with the theory of the RILW model. The simulation starts by assigning an initial velocity v_0 uniformly from $[-1, 1]$. An initial flight time τ is then generated from an exponential distribution with mean $1/|v_0|^\alpha$. In numerical simulations, the observation time is set to $t = 10^8$, and the number of particles in the sample is $n = 10^6$.

In long-time asymptotic behaviors, the MSD exhibits a power-law increase, characteristic of anomalous diffusion. Our results demonstrate excellent agreement between the numerical simulations of the IRW model and the theoretical predictions of the RILW model (see Fig. 2). Although not shown here, we confirm that numerical simulations of the RILW models with $f(v) = 1/2$ for $-1 < v < 1$ and a Gaussian model $f(v) = \mathcal{N}(0, 1)$ matches with the results of the IRW model, reinforcing the robustness of our findings. As shown in Fig. 2, as α increases beyond 1, the system transitions from normal diffusion to subdiffusion, underscoring the versatility of the model in capturing a wide range of diffusion behaviors. At $\alpha = 3/2$, an intricate balance between velocity suppression and prolonged low-velocity states minimizes spatial spreading, optimizing atomic confinement. This differs fundamentally from standard Lévy walks, where power-law-distributed flights typically lead to superdiffusion. Another transition from subdiffusion ($\gamma(\alpha) < 1$) to superdiffusion ($\gamma(\alpha) > 1$) occurs at $\alpha = 2$. Despite the mean speed approaching zero at long times, the system exhibits superdiffusion for $\alpha > 2$, reflecting the interplay between velocity suppression and long flight times.

Non-Gaussian Parameter and Deviations from Gaussian Behavior.—It is important to study deviations from

Gaussian behavior. For this purpose, we use the non-Gaussian parameter (NGP) [49], defined as

$$\text{NGP} \equiv \frac{\langle x(t)^4 \rangle}{3\langle x(t)^2 \rangle^2} - 1. \quad (15)$$

The convergence of the NGP for $t \rightarrow \infty$ implies that the fourth moment of the displacement is proportional to the square of the MSD. In purely Gaussian processes, the NGP equals zero, as all higher moments are determined solely by the second moment. A positive NGP signals a leptokurtic distribution, exhibiting a sharp central peak and heavier tails, meaning most atoms remain confined while occasional large jumps occur. Conversely, a negative NGP corresponds to a platykurtic distribution, characterized by a broader, flatter profile with more uniform spreading [50]. To compute the NGP, we calculate the fourth moment of the displacement using the Montroll-Weiss equation Eq. (10):

$$\langle \hat{x}^4(s) \rangle = \left. \frac{\partial^4}{\partial k^4} \hat{p}(k, s) \right|_{k=0}, \quad (16)$$

where $\langle \hat{x}^4(s) \rangle$ denotes the Laplace transform of $\langle x^4(t) \rangle$ with respect to time t . We then invert this expression to obtain the time-domain solution. The detailed derivation of the NGP for different regimes of α is provided in the Supplemental Material.

The behavior of the NGP across different α -regimes reveals the transition between Gaussian-like and non-Gaussian distributions (see Fig. 3). For $\alpha < 1$, the NGP approaches zero in the long-time limit, indicating a Gaussian propagator (see Supplemental Material for details). As α increases beyond 1, deviations from Gaussian behavior become pronounced due to diverging higher-order moments of the flight length. In the range $1 < \alpha < 2$, the NGP takes positive values, reflecting a highly peaked and more concentrated atomic packet. As shown in Fig. 3, at the critical point $\alpha = 3/2$, the NGP attains its peak value, indicating the most sharply peaked and concentrated propagator. This peaked propagator significantly suppresses diffusion, highlighting its relevance for atomic trapping applications. For $\alpha > 3/2$, the NGP decreases and eventually becomes negative, corresponding to a flatter distribution characteristic of ballistic spreading.

Relation with coupled CTRW.—Coupled continuous-time random walk (CTRW) theory is a phenomenological framework used to study anomalous transport, describing processes with coupled flight times and flight lengths [51]. These random processes are characterized by Montroll-Weiss equations, similar to our case. Previous work introduced an ad-hoc approach to coupled continuous-time random walks by incorporating two independent exponents [38–40]. One characterizes the coupling between flight times and jump lengths, while the other governs the statistics of jump lengths. In contrast,

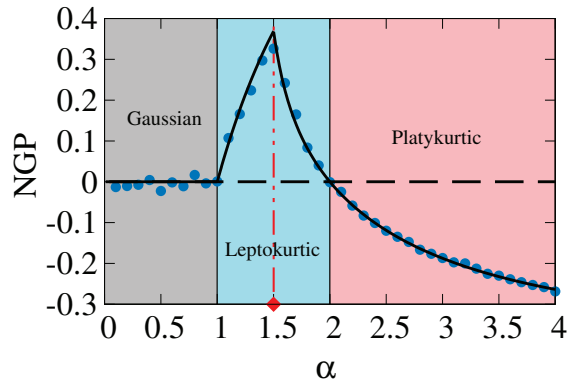


FIG. 3. Non-Gaussian parameter as a function of α . Symbols are the numerical results in the IRW model. Solid lines represent the theory of the NGP for the RILW model. To determine the non-Gaussian parameter in numerical simulations, the final decade of the observation time is used.

our model is governed by a single exponent α , yet it captures the essential physics of these coupled processes. In that sense, the approach used here is more microscopic. Interestingly, the two exponents in coupled CTRW models are actually interrelated, as they both depend on α . Our findings go far beyond traditional coupled CTRW models, revealing new insights into velocity-dependent cooling and anomalous diffusion in subrecoil-laser-cooled systems. As mentioned, the framework presented here, despite incorporating fat-tailed jump lengths and flight durations, differs significantly from the Lévy walk model. While the Lévy walk leads to either superdiffusion or normal diffusion, our approach reveals a richer spectrum of behaviors, including subdiffusion.

Conclusion.—We have demonstrated that anomalous diffusion and the shape of the propagator in subrecoil-laser-cooled atoms are tunable via the velocity-dependent fluorescence rate. By varying the parameter α , we identify the transitions between normal diffusion, subdiffusion, and superdiffusion. Our findings establish $\alpha = 3/2$ as the optimal point where diffusion is minimized due to an intricate interplay between velocity suppression and prolonged low-speed flight times. This result refines conventional Lévy walk intuition and offers a new perspective on optimizing atomic confinement. Our approach opens avenues for precision control of laser-cooled atoms, with potential applications in atomic trapping and quantum technologies.

We would like to express our deep gratitude to Prof. Günter Radons for his invaluable contributions to this work. We are deeply saddened by his recent passing. T.A. was supported by JSPS Grant-in-Aid for Scientific Research (No. C 21K033920). The support of Israel Science Foundation’s grant 1614/21 is acknowledged (EB).

* takuma@rs.tus.ac.jp

- [1] T. W. Hänsch and A. L. Schawlow, Cooling of gases by laser radiation, *Opt. Commun.* **13**, 68 (1975).
- [2] D. J. Wineland, R. E. Drullinger, and F. L. Walls, Radiation-pressure cooling of bound resonant absorbers, *Phys. Rev. Lett.* **40**, 1639 (1978).
- [3] J. Dalibard and C. Cohen-Tannoudji, Laser cooling below the doppler limit by polarization gradients: simple theoretical models, *J. Opt. Soc. Am. B* **6**, 2023 (1989).
- [4] C. N. Cohen-Tannoudji and W. D. Phillips, New mechanisms for laser cooling, *Physics Today* **43**, 33 (1990).
- [5] D. J. Wineland, C. Monroe, W. M. Itano, B. King, D. Leibfried, D. Meekhof, C. Myatt, and C. Wood, Experimental primer on the trapped ion quantum computer, *Fortschritte der Physik: Progress of Physics* **46**, 363 (1998).
- [6] S. Chu, Nobel lecture: The manipulation of neutral particles, *Rev. Mod. Phys.* **70**, 685 (1998).
- [7] C. N. Cohen-Tannoudji, Nobel lecture: Manipulating atoms with photons, *Rev. Mod. Phys.* **70**, 707 (1998).
- [8] W. D. Phillips, Nobel lecture: Laser cooling and trapping of neutral atoms, *Rev. Mod. Phys.* **70**, 721 (1998).
- [9] D. S. Weiss and M. Saffman, Quantum computing with neutral atoms, *Physics Today* **70**, 44 (2017).
- [10] H. Katori, Optical lattice clocks and quantum metrology, *Nature Photonics* **5**, 203 (2011).
- [11] M. H. Anderson, J. R. Ensher, M. R. Matthews, C. E. Wieman, and E. A. Cornell, Observation of bose-einstein condensation in a dilute atomic vapor, *Science* **269**, 198 (1995).
- [12] K. B. Davis, M. O. Mewes, M. R. Andrews, N. J. van Druten, D. S. Durfee, D. M. Kurn, and W. Ketterle, Bose-einstein condensation in a gas of sodium atoms, *Phys. Rev. Lett.* **75**, 3969 (1995).
- [13] I. Bloch, J. Dalibard, and S. Nascimbene, Quantum simulations with ultracold quantum gases, *Nat. Phys.* **8**, 267 (2012).
- [14] F. Bardou, J.-P. Bouchaud, A. Aspect, and C. Cohen-Tannoudji, *Lévy statistics and laser cooling: how rare events bring atoms to rest* (Cambridge University Press, 2002).
- [15] G. Afek, N. Davidson, D. A. Kessler, and E. Barkai, Colloquium: Anomalous statistics of laser-cooled atoms in dissipative optical lattices, *Rev. Mod. Phys.* **95**, 031003 (2023).
- [16] F. Bardou, J. P. Bouchaud, O. Emile, A. Aspect, and C. Cohen-Tannoudji, Subrecoil laser cooling and lévy flights, *Phys. Rev. Lett.* **72**, 203 (1994).
- [17] T. Esslinger, F. Sander, M. Weidemüller, A. Hemmerich, and T. W. Hänsch, Subrecoil laser cooling with adiabatic transfer, *Phys. Rev. Lett.* **76**, 2432 (1996).
- [18] B. Saubaméa, M. Leduc, and C. Cohen-Tannoudji, Experimental investigation of nonergodic effects in subrecoil laser cooling, *Phys. Rev. Lett.* **83**, 3796 (1999).
- [19] E. Barkai, G. Radons, and T. Akimoto, Transitions in the ergodicity of subrecoil-laser-cooled gases, *Phys. Rev. Lett.* **127**, 140605 (2021); Gas of subrecoiled laser cooled atoms described by infinite ergodic theory, *J. Chem. Phys.* **156** (2022).
- [20] A. Aspect, E. Arimondo, R. Kaiser, N. Vansteenkiste, and C. Cohen-Tannoudji, Laser cooling below the one-

- photon recoil energy by velocity-selective coherent population trapping, *Phys. Rev. Lett.* **61**, 826 (1988).
- [21] M. Kasevich and S. Chu, Laser cooling below a photon recoil with three-level atoms, *Phys. Rev. Lett.* **69**, 1741 (1992).
- [22] N. Davidson, H. J. Lee, M. Kasevich, and S. Chu, Raman cooling of atoms in two and three dimensions, *Phys. Rev. Lett.* **72**, 3158 (1994).
- [23] S. Marksteiner, K. Ellinger, and P. Zoller, Anomalous diffusion and lévy walks in optical lattices, *Phys. Rev. A* **53**, 3409 (1996).
- [24] E. Curtis, C. W. Oates, and L. Hollberg, Quenched narrow-line laser cooling of 40 ca to near the photon recoil limit, *Physical Review A* **64**, 031403 (2001).
- [25] O. N. Prudnikov and E. Arimondo, Sub-doppler laser cooling on combined optical transitions, *J. Opt. Soc. Am. B* **20**, 909 (2003).
- [26] T. Geisel, J. Nierwetberg, and A. Zacherl, Accelerated diffusion in josephson junctions and related chaotic systems, *Phys. Rev. Lett.* **54**, 616 (1985).
- [27] S. V. Buldyrev, A. L. Goldberger, S. Havlin, C.-K. Peng, M. Simons, and H. E. Stanley, Generalized lévy-walk model for dna nucleotide sequences, *Phys. Rev. E* **47**, 4514 (1993).
- [28] G. Ramos-Fernández, J. L. Mateos, O. Miramontes, G. Cocho, H. Larralde, and B. Ayala-Orozco, Lévy walk patterns in the foraging movements of spider monkeys (*ateles geoffroyi*), *Behavioral ecology and Sociobiology* **55**, 223 (2004).
- [29] J. Klafter and I. M. Sokolov, Anomalous diffusion spreads its wings, *Phys. World* **18**, 29 (2005).
- [30] P. Barthelemy, J. Bertolotti, and D. S. Wiersma, A lévy flight for light, *Nature* **453**, 495 (2008).
- [31] P. Dieterich, R. Klages, R. Preuss, and A. Schwab, Anomalous dynamics of cell migration, *Proc. Natl. Acad. Sci. USA* **105**, 459 (2008).
- [32] V. Zaburdaev, S. Denisov, and J. Klafter, Lévy walks, *Rev. Mod. Phys.* **87**, 483 (2015).
- [33] M. S. Song, H. C. Moon, J.-H. Jeon, and H. Y. Park, Neuronal messenger ribonucleoprotein transport follows an aging lévy walk, *Nature communications* **9**, 1 (2018).
- [34] A. G. Cherstvy, O. Nagel, C. Beta, and R. Metzler, Non-gaussianity, population heterogeneity, and transient superdiffusion in the spreading dynamics of amoeboid cells, *Phys. Chem. Chem. Phys.* **20**, 23034 (2018).
- [35] J. Klafter, A. Blumen, and M. F. Shlesinger, Stochastic pathway to anomalous diffusion, *Phys. Rev. A* **35**, 3081 (1987).
- [36] M. F. Shlesinger, B. J. West, and J. Klafter, Lévy dynamics of enhanced diffusion: Application to turbulence, *Phys. Rev. Lett.* **58**, 1100 (1987).
- [37] T. Albers and G. Radons, Exact results for the non-ergodicity of d -dimensional generalized lévy walks, *Phys. Rev. Lett.* **120**, 104501 (2018); Nonergodicity of d -dimensional generalized lévy walks and their relation to other space-time coupled models, *Phys. Rev. E* **105**, 014113 (2022).
- [38] T. Akimoto and T. Miyaguchi, Distributional ergodicity in stored-energy-driven lévy flights, *Phys. Rev. E* **87**, 062134 (2013).
- [39] T. Akimoto and T. Miyaguchi, Phase diagram in stored-energy-driven lévy flights, *J. Stat. Phys.* **157**, 515 (2014).
- [40] P. Zhu, Y. Hu, and J. Liu, Asymmetric space-time correlated continuous-time random walk, *The European Physical Journal B* **96**, 66 (2023).
- [41] E. Bertin and F. Bardou, From laser cooling to aging: a unified lévy flight description, *American Journal of Physics* **76**, 630 (2008).
- [42] A. L. Gaunt, T. F. Schmidutz, I. Gotlibovych, R. P. Smith, and Z. Hadzibabic, Bose-einstein condensation of atoms in a uniform potential, *Phys. Rev. Lett.* **110**, 200406 (2013).
- [43] A. Aspect, E. Arimondo, R. Kaiser, N. Vansteenkiste, and C. Cohen-Tannoudji, Laser cooling below the one-photon recoil energy by velocity-selective coherent population trapping: theoretical analysis, *J. Opt. Soc. Am. B* **6**, 2112 (1989).
- [44] J. Reichel, F. Bardou, M. B. Dahan, E. Peik, S. Rand, C. Salomon, and C. Cohen-Tannoudji, Raman cooling of cesium below 3 nk: New approach inspired by lévy flight statistics, *Phys. Rev. Lett.* **75**, 4575 (1995).
- [45] E. W. Montroll and G. H. Weiss, Random walks on lattices. ii, *Journal of Mathematical Physics* **6**, 167 (1965).
- [46] M. Shlesinger, J. Klafter, and Y. Wong, Random walks with infinite spatial and temporal moments, *J. Stat. Phys.* **27**, 499 (1982).
- [47] T. Akimoto, E. Barkai, and G. Radons, Infinite invariant density in a semi-markov process with continuous state variables, *Phys. Rev. E* **101**, 052112 (2020).
- [48] R. Metzler and J. Klafter, The random walk's guide to anomalous diffusion: a fractional dynamics approach, *Phys. Rep.* **339**, 1 (2000).
- [49] A. Rahman, Correlations in the motion of atoms in liquid argon, *Physical review* **136**, A405 (1964).
- [50] I. Marchenko, I. Marchenko, J. Luczka, and J. Spiechowicz, Approach to nonequilibrium: From anomalous to brownian diffusion via non-gaussianity, *Chaos: An Interdisciplinary Journal of Nonlinear Science* **35** (2025).
- [51] M. Dentz, H. Scher, D. Holder, and B. Berkowitz, Transport behavior of coupled continuous-time random walks, *Physical Review E—Statistical, Nonlinear, and Soft Matter Physics* **78**, 041110 (2008).
- [52] V. Zaburdaev, S. Denisov, and J. Klafter, Lévy walks, *Reviews of Modern Physics* **87**, 483 (2015).

Supplemental Material for *Transitions in Anomalous Diffusion of Subrecoil-Laser-Cooled Atoms*

Derivation of the mean square displacement at $\alpha = 1.5$

Here, we compute the exact asymptotic behavior of the mean square displacement (MSD) at $\alpha = 1.5$. At this parameter, the second moment of flight length diverges. The time-dependent second moment is given by

$$\int_{-\infty}^{\infty} x^2 \psi(x, t) dx = \frac{1}{t^{1+\alpha}} \int_0^t x^{2+\alpha} e^{-x^\alpha t^{1-\alpha}} dx. \quad (17)$$

Using the change of variables ($y = x^\alpha t^{1-\alpha}$), this transforms into

$$\int_{-\infty}^{\infty} x^2 \psi(x, t) dx = \frac{\gamma(\frac{3}{\alpha} + 1, t)}{\alpha} t^{1-\frac{3}{\alpha}}, \quad (18)$$

where $\gamma(a, t)$ is the lower incomplete gamma function. For $\alpha = 1.5$, the integral simplifies to

$$\int_{-\infty}^{\infty} x^2 \psi(x, t) dx = \frac{2\gamma(3, t)}{3} t^{-1}. \quad (19)$$

In the asymptotic limit $t \rightarrow \infty$, the incomplete gamma function approaches $\Gamma(3) = 2$, leading to

$$\int_{-\infty}^{\infty} x^2 \psi(x, t) dx \sim \frac{4}{3} t^{-1}. \quad (20)$$

Thus, the asymptotic behavior of the time-integrated second moment is

$$\int_0^t dt' \int_{-\infty}^{\infty} x^2 \psi(x, t') dx \sim \frac{4}{3} \ln t. \quad (21)$$

The Laplace transform of the MSD is given by

$$\langle \hat{x}^2(s) \rangle = - \left. \frac{\hat{\Psi}''(k, s)}{1 - \hat{\psi}(k, s)} \right|_{k=0} - \left. \frac{\hat{\Psi}(k, s) \hat{\psi}''(k, s)}{[1 - \hat{\psi}(k, s)]^2} \right|_{k=0}. \quad (22)$$

The leading term in the asymptotic regime is

$$\langle \hat{x}^2(s) \rangle \sim - \frac{4 \ln(1/s)}{3a s^{1+1/\alpha}}. \quad (23)$$

where $a = \frac{\pi \csc(\pi/\alpha)}{\alpha}$ is derived from the flight-time statistics. Transforming back to the time domain, the asymptotic behavior of the MSD becomes

$$\langle x^2(t) \rangle \sim \frac{4 \ln t}{3a \Gamma(5/3)} t^{\frac{2}{3}}. \quad (24)$$

Numerical simulations of the IRW model: Dependence of σ on the MSD

The simulation starts by assigning an initial velocity v_0 uniformly from $[-1, 1]$. To prevent unbounded velocity changes, reflecting walls are imposed, ensuring the velocity is bounded. The total particle position $x(t)$ is updated iteratively as

$$x(t) = \sum_{i=0}^{N_t} v_i \tau_i + (t - N_t) v_{N_t+1} \tau_{N_t+1}, \quad (25)$$

where N_t is the number of velocity changes until time t . An initial flight time τ_0 is then generated from an exponential distribution with mean $1/|v_0|^\alpha$. During this flight, the velocity remains constant, and the particle's displacement is

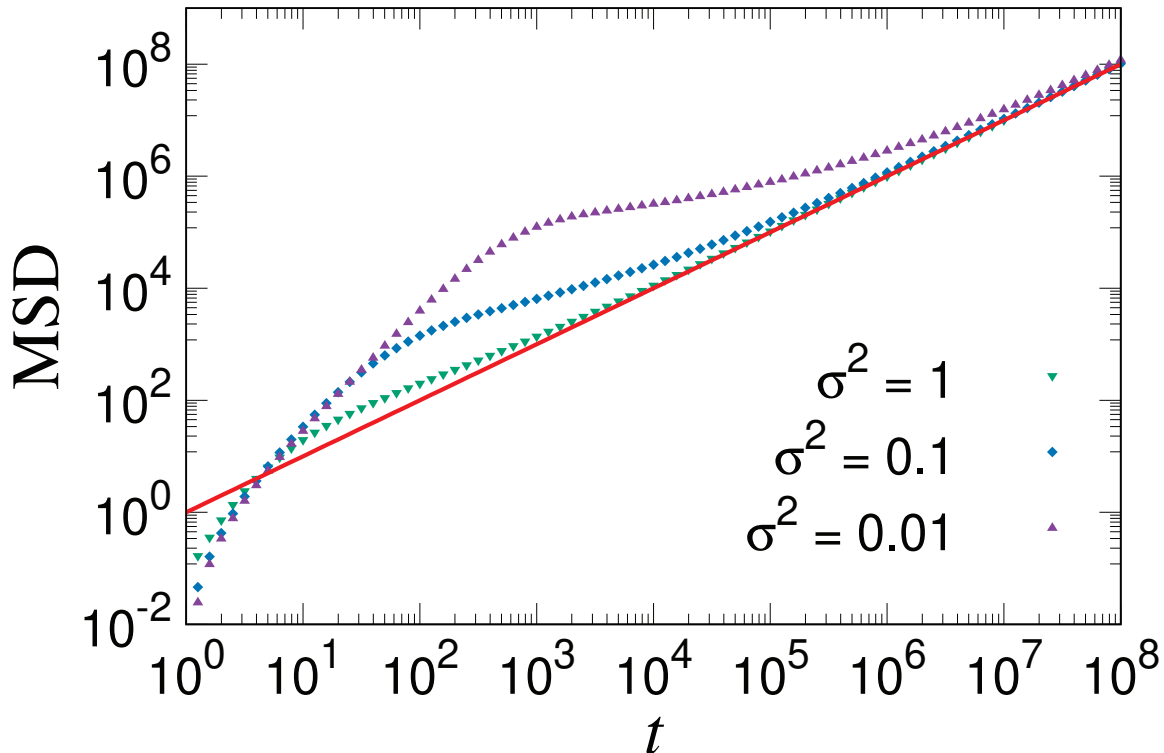


FIG. 4. MSD dependence on σ for $\alpha = 2$. MSD is compared for three variance parameters: $\sigma^2 = 1, 0.1, 0.01$. The red solid line represents the values obtained from theoretical calculations. In the short-time regime, the MSD differs depending on the value of σ , while in the long-time regime, all curves converge to the same value.

calculated as $\Delta x = v_0 \tau_0$. After the flight time ends, the velocity is updated to $v_1 = v_0 + \Delta v$, where Δv is sampled from a Gaussian distribution $\mathcal{N}(0, 1)$.

The variance σ^2 in the Gaussian distribution affects the MSD in the intermediate regime, where the MSD exhibits the crossover time from t^2 to $t^{\gamma(\alpha)}$. However, as shown in Fig. 4, we confirm that the same power-law exponent $\gamma(\alpha)$ in the MSD is obtained for $\sigma^2 = 1, 0.1$, and 0.01 in the long-time regime. Figure 4 shows the dependence of the MSD on the variance parameter σ for cold atoms, assuming Gaussian-distributed jumps. The MSD is plotted for three different values of σ^2 : 1, 0.1, and 0.01. The red solid line represents the theoretical predictions from Eq. (14).

In the short-time regime ($t < 10$), the MSD grows faster than ballistic scaling (t^2), indicating an accelerated spreading of particles. This rapid initial increase is more pronounced for larger variance σ^2 , as higher variance increases the probability of particles having greater initial speeds, enabling them to make larger jumps and expand over a wider range in a short time.

In the intermediate-time regime ($t > 10$), the ordering of the MSD curves reverses, meaning that the MSD becomes larger for smaller σ^2 . This reversal occurs because particles with initially high speed (in cases with large σ^2) become trapped near zero momentum earlier, suppressing their movement. In contrast, when σ^2 is small, particles maintain moderate momentum over a longer period, resulting in a higher MSD in this regime.

In the long-time regime, all MSD curves converge to the same value regardless of σ , indicating that the system ultimately reaches a universal diffusive behavior.

Derivation of the non-Gaussian parameter

To obtain the non-Gaussian parameter (NGP) analytically, we derive the fourth moment of the displacement. The Laplace transform of the survival probability $\Psi(t)$ is defined as

$$\hat{\Psi}(s) = \int_0^{\infty} \Psi(t) e^{-st} dt. \quad (26)$$

For $\alpha < 1$, it becomes

$$\hat{\Psi}(0) = \int_0^{\infty} \Psi(t) dt = \int_0^{\infty} t\psi(t) dt = \mu, \quad (27)$$

where μ is the mean flight time, which is finite. Using Eq. (11) and the inverse Laplace transform yields the asymptotic behavior of the MSD for $t \rightarrow \infty$:

$$\langle x(t)^2 \rangle \sim \frac{\langle \Delta x^2 \rangle}{\mu} t. \quad (28)$$

Furthermore, the asymptotic behavior of the fourth moment of the displacement for $t \rightarrow \infty$ is also calculated as

$$\langle x(t)^4 \rangle \sim \frac{3\langle \Delta x^2 \rangle^2}{\mu^2} t^2. \quad (29)$$

Thus, the NGP becomes zero for $\alpha < 1$.

The leading order of the 4th moment for $\alpha < 3/2$ is given by

$$\langle x(t)^4 \rangle \sim \frac{6\langle \Delta x^2 \rangle^2}{a^2 \Gamma(1 + \frac{2}{\alpha})} t^{\frac{2}{\alpha}} \quad (t \rightarrow \infty). \quad (30)$$

Therefore, the 4th moment is proportional to the square of the second moment, i.e., $t^{\frac{2}{\alpha}}$. For $1 < \alpha < 3/2$, the NGP approaches

$$\text{NGP} \rightarrow \frac{2\Gamma(1 + \frac{1}{\alpha})^2}{\Gamma(1 + \frac{2}{\alpha})} - 1 \quad (t \rightarrow \infty). \quad (31)$$

For $\alpha > 3/2$, the 4th moment becomes

$$\begin{aligned} \langle x(t)^4 \rangle &\sim \left(\frac{\Gamma(\frac{5}{\alpha}) \Gamma(5 - \frac{5}{\alpha})}{a\alpha} + \frac{6\Gamma(\frac{3}{\alpha}) \Gamma(3 - \frac{3}{\alpha}) \Gamma(\frac{3}{\alpha} + 1) \Gamma(2 - \frac{3}{\alpha})}{a^2 \alpha^2} \right. \\ &\quad \left. + \frac{\Gamma(\frac{5}{\alpha} + 1) \Gamma(4 - \frac{5}{\alpha})}{a\alpha} + \frac{6\Gamma(\frac{3}{\alpha} + 1)^2 \Gamma(2 - \frac{3}{\alpha})^2}{a^2 \alpha^2} \right) \frac{t^{4 - \frac{4}{\alpha}}}{\Gamma(5 - \frac{4}{\alpha})} \quad (t \rightarrow \infty) \\ &= \frac{4 \sin^2(\frac{\pi}{\alpha}) [9(\alpha - 3)^2 \csc^2(\frac{3\pi}{\alpha}) + (\alpha - 5)(2\alpha - 5)(3\alpha - 5) \csc(\frac{\pi}{\alpha}) \csc(\frac{5\pi}{\alpha})]}{\alpha^3 \Gamma(5 - \frac{4}{\alpha})} t^{4 - \frac{4}{\alpha}}. \end{aligned} \quad (32)$$

The asymptotic behavior of the NGP becomes

$$\text{NGP} \rightarrow \frac{\Gamma(3 - \frac{2}{\alpha})^2 [9(\alpha - 3)^2 + (\alpha - 5)(2\alpha - 5)(3\alpha - 5) \sin^2(\frac{3\pi}{\alpha}) \csc(\frac{\pi}{\alpha}) \csc(\frac{5\pi}{\alpha})]}{3(\alpha - 3)^2 \alpha \Gamma(5 - \frac{4}{\alpha})} - 1 \quad (t \rightarrow \infty). \quad (33)$$

Details of $\langle \Delta x^2 \rangle$

The second moment of flight length $\langle \Delta x^2 \rangle$ is given by

$$\langle \Delta x^2 \rangle = \int_{-\infty}^{\infty} x^2 \varphi(x) dx. \quad (34)$$

Because the asymptotic behavior of $\varphi(x)$ is given by

$$\varphi(x) \propto x^{-\frac{\alpha}{\alpha-1}} \quad (35)$$

for $x \rightarrow \infty$. It diverges for $\alpha \geq 3/2$.